Author's Version

Microstructure and cyclic oxidation resistance of Si-aluminide coatings on γ-TiAl at 850 °C

R. Swadźba[a,1], L. Swadźba[2], B. Mendala[2], Peter-Philipp Bauer[3] Nadine Laska[3], Uwe Schulz[3]

[1]Łukasiewicz Research Network - Institute for Ferrous Metallurgy, Gliwice, Poland

[2]Silesian University of Technology, Gliwice, Poland

[3]DLR German Aerospace Center, Cologne, Germany

[a]Corresponding author

Email address: rswadzba@gmail.com

KEYWORDS: γ-TiAl, High Temperature Oxidation, Intermetallics

ABSTRACT

The paper concerns the deposition and high temperature oxidation behavior of simple aluminide and SiAl coatings on the TiAl-based alloy TNB-V5. The coatings were produced using pack cementation method with varying content of Si and Al in the pack. The samples were thermally cycled at 850 °C in 23 h cycles up to 131 cycles (total of 3013 hours) in order to obtain mass change curves. The results of cyclic oxidation tests were related to the microstructure of the as deposited coatings. Special effort has been done in order to study the growth of protective oxide scales as well as the evolution of the metal-scale interfaces in detail using analytical high resolution Scanning Transmission Electron Microscopy (STEM).

1. Introduction

TiAl-based alloys have been successfully implemented in the automotive [1,2] as well as aircraft industries due to their excellent properties such as low density and high specific strength [3–5]. These materials have been of great interest for aircraft engine manufacturers, such as

General Electric, Pratt & Whitney and Rolls-Royce [3,6] as a light-weight alternative for Ni-based superalloys [7–9].

Depending on the chemical composition of the alloy the maximum operating temperatures of these materials in air can vary between 750 – 850 °C [10], above which excessive oxidation occurs and the mechanical properties, such as creep and tensile strength, decrease. The former is related to the formation of non-protective oxide scales, consisting of a mixture of titania and alumina, along with the formation of TiN/Ti_2A1N or Ti_3AlN nitrides at the metal-scale interface [11–14]. Such scales do not serve as a diffusion barrier for oxygen and their growth leads to high mass gains in addition to dissolution of oxygen, and presumably nitrogen, in the substrate alloy [7,12]. The latter leads to deterioration of both room and high temperature mechanical properties [12].

Over the years extensive efforts have been made in order to extend the lifetimes of TiAl alloys at high temperatures. They involved surface engineering techniques devoted to deposition of various oxidation resistant coatings as well as bondcoatings for Thermal Barrier Coating systems. Various testing temperatures were targeted starting from 800 °C [15–17], 850 °C [18,19], 900 °C [20–22], 950 °C [19,20,23–26] up to 1000 °C and above [27–30]. Numerous coating deposition technologies have been studied, including pack cementation [19], slurry aluminizing [25,26], vapor phase aluminizing [26,31,32], halogen effect [33–36] and PVD [23,24,37–40]. Some of these works involved also deposition of bondcoatings and application of Thermal Barrier Coatings [31,36,37,41,42]. The SiAl coatings studied in the past involved the application of slurry methods (12.5 wt. % Si and Al) [25], pack cementation method [19] or Arc-PVD (11 wt. % Si and Al) [23,24]. However, these works did not focus on the metal-scale interface evolution and oxide scale growth during the cyclic oxidation at 850 °C.

This paper presents the results of investigations of the Si effect on the growth of aluminide coatings on TNB-V5 alloy as well as its influence on the oxidation behavior at 850 °C. The

paper focuses on the detailed microstructural investigations using analytical Scanning Transmission Electron Microscopy (STEM) of the metal-scale interfaces and oxide scales formed on the coatings during the cyclic oxidation test.

2. Experimental Procedure

The investigated material was the TNB-V5 alloy with chemical composition Ti-45Al-5Nb-0.2B-0.2C (all in at. %). It was produced using extrusion in the form of rods with ø20 mm of diameter and length of 200 mm. The material was subjected to a heat treatment consisting of annealing at 1250°C for 1 hour and then at 850 °C for 6 hours. The rods were cut to coupons with dimensions of ø20 x 4 mm and then ground using 500 grit paper. Simple aluminide coatings (Si-free) were obtained using diffusion aluminizing by the pack cementation method with the application of NH_4Cl activator and a proprietory Al containing powder (ACP). The SiAl coatings were obtained by applying various mixtures of pure Si powder and ACP, named low-Si (80 wt. % Si) and high-Si (90 wt. % Si). The coating deposition processes were performed at 850 °C for a duration of 6h. The coated samples were subjected to the cyclic oxidation test in laboratory air at 850 °C in 23 hour cycles. Three samples were tested for each condition and curves of average mass changes versus amount of 23 hour cycles were plotted. After every cycle the samples were cooled down to room temperature, weighted using an analytical balance and returned to the furnace. After the cyclic oxidation test the microstructure of the samples was investigated using a Field Emission Gun (FEG) equipped Scanning Electron Microscope (SEM) FEI INSPECT F equipped with EDS and EBSD detectors by EDAX. All the EDS results are shown as an average of the area measurements. The high resolution investigations of the coatings as well as oxide scales formed during high temperature oxidation experiments were performed using a Cs-corrected Scanning Transmission Electron Microscope (STEM) FEI TITAN 80-300 operating at 300 kV using Z-sensitive High Angle Annular Dark Field (HAADF) and Annular Dark Field (ADF) detectors. The chemical composition of the

oxidation products was studied using Energy Dispersive Spectroscopy (EDS) and Electron Energy Loss Spectroscopy (EELS) under STEM mode. The samples for STEM investigations were prepared using Focused Ion Beam (FIB) on a FEI Quanta 3D 200i dual-beam system. During the FIB preparation of samples Pt layers (15 µm x 2 µm x 2 µm) were applied on top of the samples to protect them during the gallium ion thinning process. The phase composition of the samples after coating deposition and after the cyclic oxidation test was studied using X-ray diffraction method applying PANanalytical Empyrean system with cobalt and copper X-ray sources. The XRD results are plotted as d-spacing vs square root of counts to highlight the low-intensity peaks.

3. Results and Discussion

3.1. Characterization of the base alloy

The SEM-BSE image of the investigated TNB-V5 alloy along with its phase composition analysis using EBSD are shown in Fig. 1a-c. As shown in the EBSD phase (Fig. 1b) and orientation maps (Fig. 1c) the alloy's microstructure is characterized by the presence of large lamellar colonies containing alternately stacked γ-TiAl and α_2-Ti_3Al lamellas without any β-Ti grains. Quantitative EBSD analysis revealed that the alloy contains around 72 vol.-% γ-TiAl, and 28 vol.-% α_2-Ti_3Al phase.

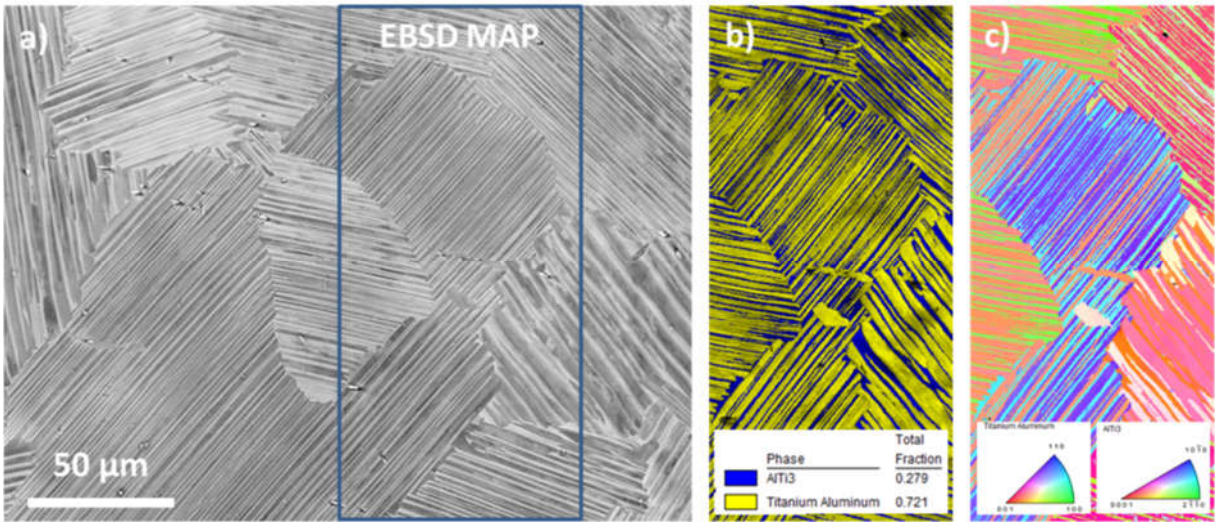

Fig. 1. Microstructure of the investigated TNB-V5 alloy: SEM-BSE (a), EBSD phase map (b) and c) EBSD orientation map.

3.2. Characterization of as-deposited coatings

The SEM-BSE images of the cross-sectional microstructures as well as XRD patterns of the as-deposited simple, low-Si and high-Si SiAl coatings are shown in Figs. 2-4 along with chemical composition analyses results shown in Tab. 1-3.

The simple aluminide coating obtained using 100% ACP without the application of silicon was characterized by thickness of around 8 μm (Fig. 2a) and presence of two distinctive zones and an additional Al-enriched zone in the substrate alloy. The outer zone of the coating is composed of Al-rich grains (area 1 in Fig. 2b and Tab. 1) containing around 74 at. % of Al and 23 at. % of Ti with balance of Nb. Based on the XRD results it is most likely the $TiAl_3$ phase (Fig. 2c). It is noteworthy, that the bright layer on top of the coating's cross-section originates from charging effect under SEM. Directly underneath it there is a zone marked as 2 in Fig. 2b containing around 68 at. % Al (point 2 in Tab. 1), which most likely corresponds to the $TiAl_2$ phase, as shown in the XRD results shown in Fig. 2c. Underneath the coating there is a thin layer of γ-TiAl phase enriched in Al (marked as 3 in Fig. 2b and Tab. 1) that contains around 52 at. % of Al which is 5 at. % higher compared to the lamellar area in the substrate alloy marked as 4 in Fig. 2b and Tab. 1.

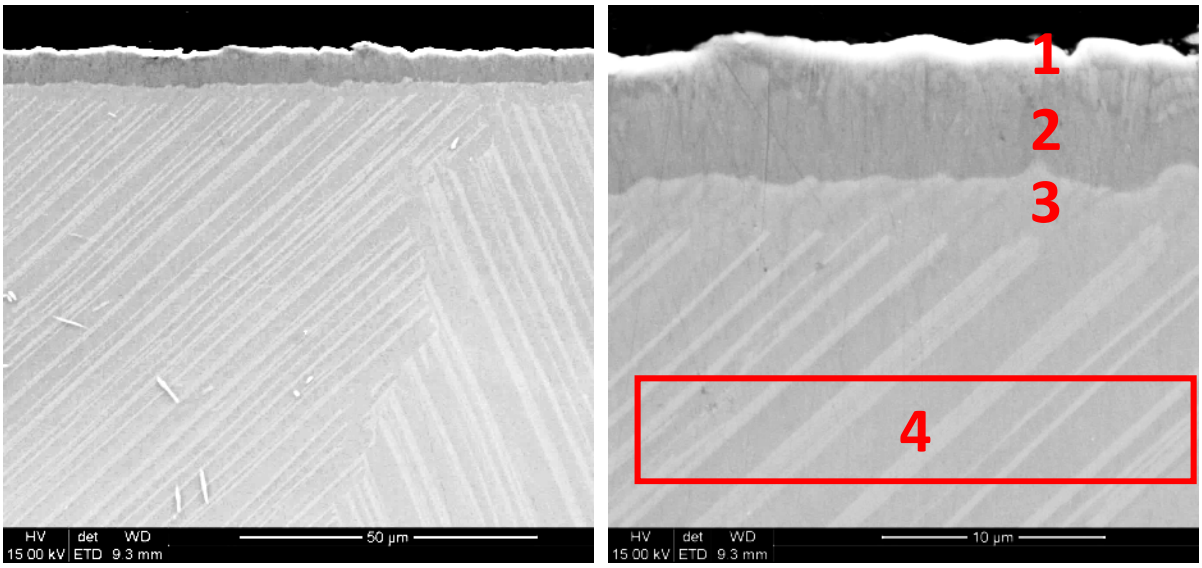

a) b)

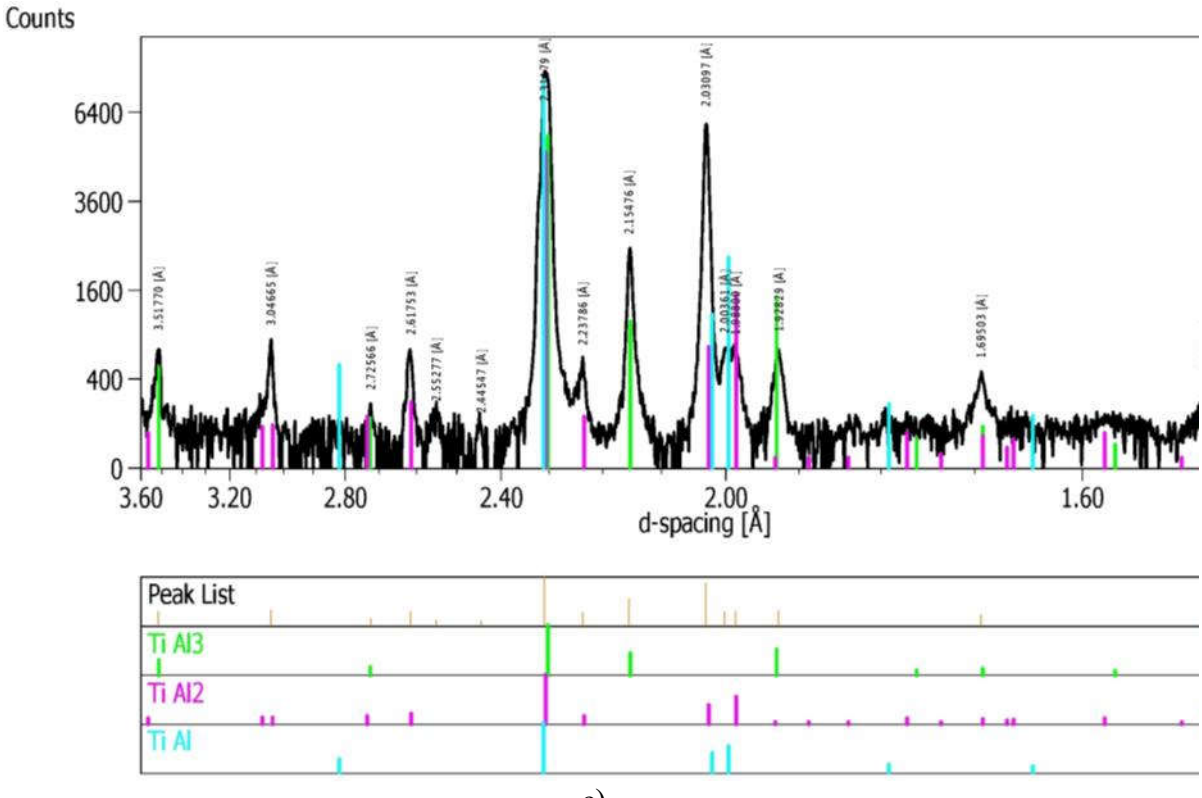

c)

Figure 2 Cross-sectional microstructure of simple aluminide coating on TiAl (a,b) along with XRD pattern from the surface (c).

Table 1 Chemical composition of microareas marked in Fig. 2b.

	1		2		3		4	
	wt. %	at. %	wt. %	at. %	wt. %	at. %	wt. %	at. %
Al	58,6	73,8	51,7	67,8	35,7	52,3	31,3	47,3
Nb	9,3	3,4	9,8	3,7	13,4	5,7	14,0	6,2
Ti	32,1	22,8	38,5	28,5	50,9	42,0	54,7	46,6

The application of the pack cementation process where a high amount of silicon powder is mixed with ACP (high-Si coating) results in the formation of a much thicker coating compared to the simple Si-free aluminide coating (obtained with 100 % ACP). The coating is around 26 µm thick (Fig. 3a) which indicates a threefold increase in coating growth rate in the presence of Si in the pack. Moreover, the coating consists of two layers, among which the outer one is around 95% of the whole coating thickness. The outer layer that is 24 µm thick contains around 75 at. % of Al as well as 23 at. % Ti and balance of Nb (Fig. 3a, Tab 2). Based on the XRD results shown in Fig. 3 it is most likely the $TiAl_3$ phase. At the interface with the substrate alloy there is a thin (around 1.5 µm) zone containing around 65 at. % of Al as well as 30 at. % Ti and trace amounts of Nb, which corresponds to the $TiAl_2$ phase found by XRD (Fig. 3c). Moreover, the lower portion of the outer $TiAl_3$ zone as well as the $TiAl_2$ zone contain numerous very fine precipitates that appear bright in the SEM-BSE image, marked as 3 in Fig. 3b. Based on the increased amount of Si in these precipitates, as shown in chemical composition analysis results in Tab. 2 (point 3) it is plausbile to conclude that these are Ti silicide precipitates. However, due to their presence mostly at the metal-coating interface it was not possible to identify them using XRD. The additional peak corresponding to the Ti_3Al phase in the XRD pattern is most probably coming from the substrate alloy.

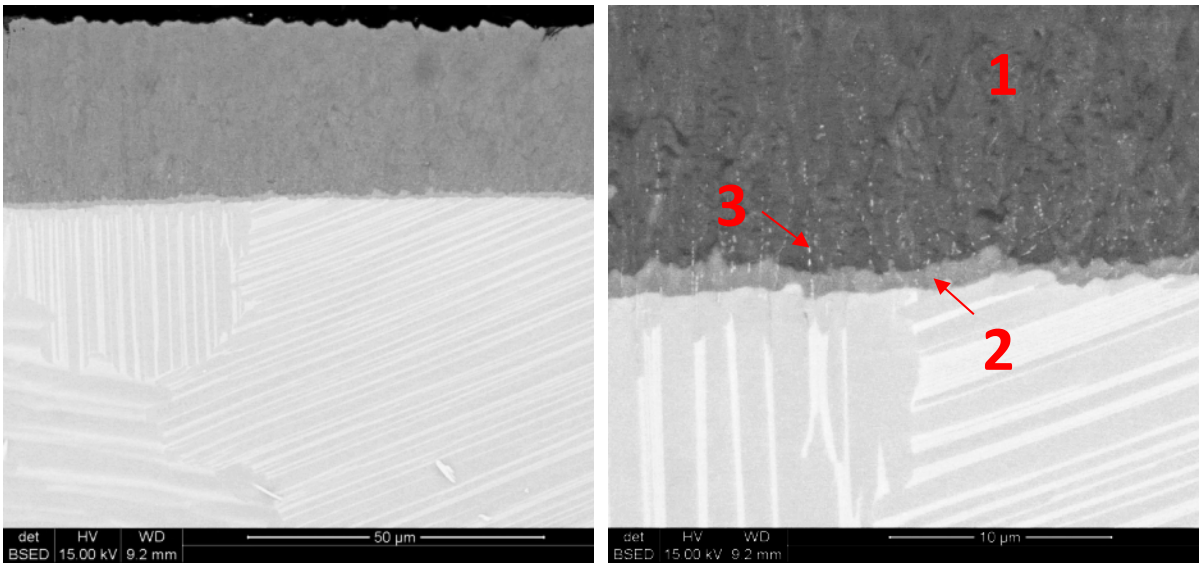

a) b)

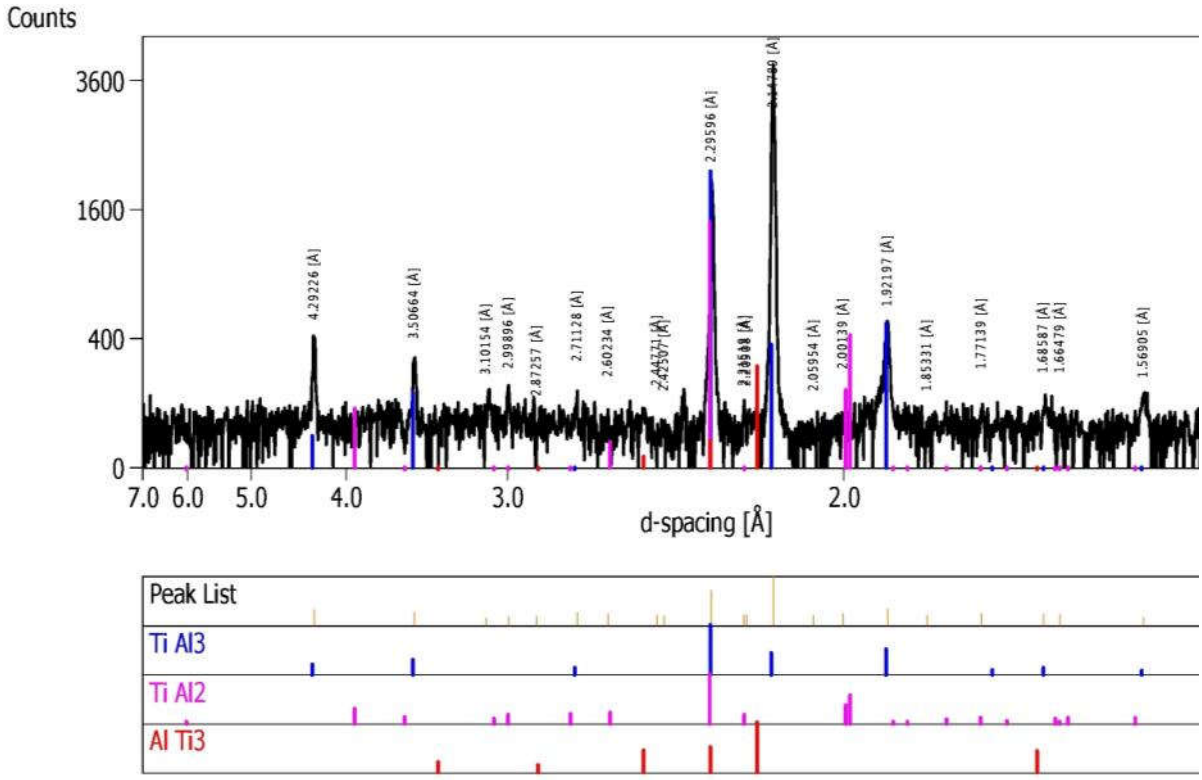

c)

Figure 3 Cross-sectional microstructure of the high-Si SiAl coating on TiAl (a,b) along with XRD pattern from the surface (c).

Table 2 Chemical composition in microareas marked in Fig. 3b.

	1		2		3	
	wt. %	at. %	wt. %	at. %	wt. %	at. %
Al	59,8	74,4	48,6	65,2	38,5	50,7
Si					13,3	16,8
Nb	7,4	2,7	11	4,3	8,9	3,4
Ti	32,8	23	40,4	30,5	39,3	29,2

Increasing the amount of ACP powder in the pack composition leads to the formation of a low-Si aluminide coating characterized by distinct differences in the microstructure and composition. The coating shown in Fig. 4. is measurably thicker – around 36 µm (Fig. 4a), compared to the high-Si coating (Fig. 3b). However, the microstructure of the coating is very similar to the previously described one. As evidenced using EDS (Tab. 3) and XRD (Fig. 4c) the coating is characterized by the presence of the outer $TiAl_3$ zone containing around 75 at. %

of Al, 23 at. % of Ti as well as trace amounts of Nb (area 1 in Fig. 4b and Tab. 3). Moreover, the thickness ratio of the outer $TiAl_3$ and inner $TiAl_2$ (area 2 in Fig. 4b and Tab. 3) zones is similar as well. The major difference between the low- and high-Si aluminide coatings is the amount of silicides precipitates both in the outer and inner zones of the coatings. As can be expected, the application of a lower amount of silicon powder leads to a decrease in the amount of silicides to the level where XRD analysis does not detect them (Fig. 4c). As a matter of fact only $TiAl_3$ and $TiAl_2$ phases were detected along with Ti_3Al from the substrate alloy. Based on the SEM observations in the low-Si coating it is possible to distinguish very fine bright precipitates at the interface between the coating and the substrate (Fig. 4b). However, additional STEM-HAADF imaging was necessary to study the coating's substructure. These investigations concerned the outer region of the coating, marked as 1 in Fig. 4a, as well as the interface between the coating ($TiAl_3$ / $TiAl_2$) and the substrate, marked as 2 in Fig. 4b. As shown in Fig. 5 the outer zone of the coating contains numerous nanometric sized (around 25-50nm), round titanium silicides distributed within the grains of the $TiAl_3$ phase (Fig. 5b,c,d) along with dislocations bending around them. The elemental mapping shown in Fig. 5c-f indicates that Si is present only in the precipitates along with Ti, while almost no signal of this element is present in the surrounding $TiAl_3$ phase. Moreover, Al is depleted in the silicides precipitates, while Nb is distributed uniformly in the studied area. The interface between the coating and the substrate is shown in Fig. 6. The STEM-HAADF image in Fig. 6a illustrates that the majority of the titanium silicides is present directly above the $TiAl_2$ phase layer in form of elongated precipitates and also on the grain boundaries of the $TiAl_2$ grains. As shown in Fig. 6b these silicides were identified as Ti_5Si_3. The elemental mappings shown in Fig. 6c-f illustrate the distribution of Si, which is segregated solely to the titanium silicides, as well as the gradient in Ti distribution from the $TiAl_3$ through $TiAl_2$ to the substrate TiAl alloy. An opposite gradient of concentration can be observed for Al which increases towards the coating. The distribution

of Nb indicates that the highest concentration of this element is present in the substrate alloy with just trace amounts within the coating.

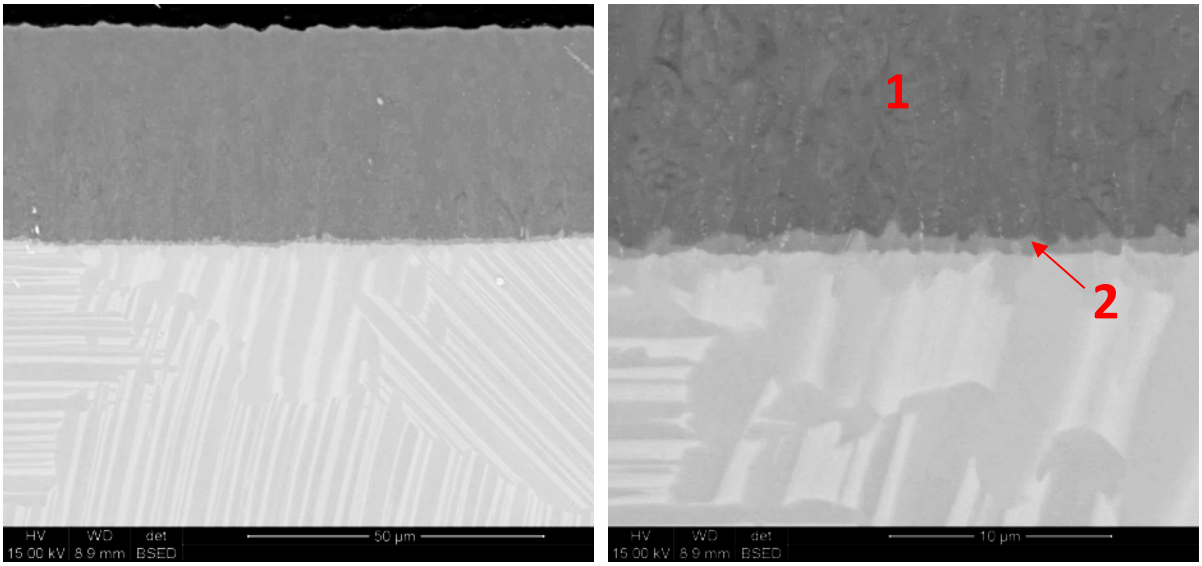

a) b)

c)

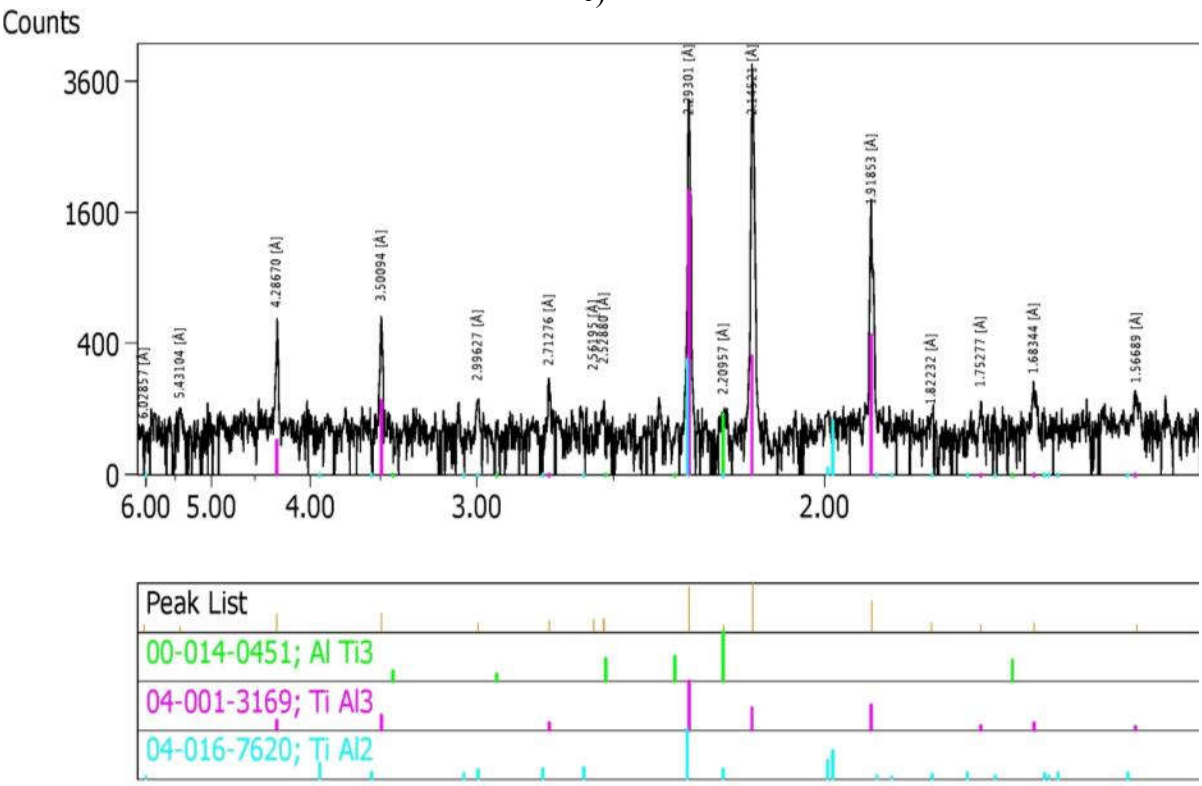

Figure 4 Cross-sectional microstructure of low-Si SiAl coating on TiAl (a,b) along with XRD pattern (c).

Table 3 Chemical composition in microareas marked in Fig. 4b.

	1		2	
	wt. %	at. %	wt. %	at. %
Al	61,6	75,6	49,1	65,6
Nb	6,6	2,4	10,5	4,1
Ti	31,8	22,0	40,4	30,4

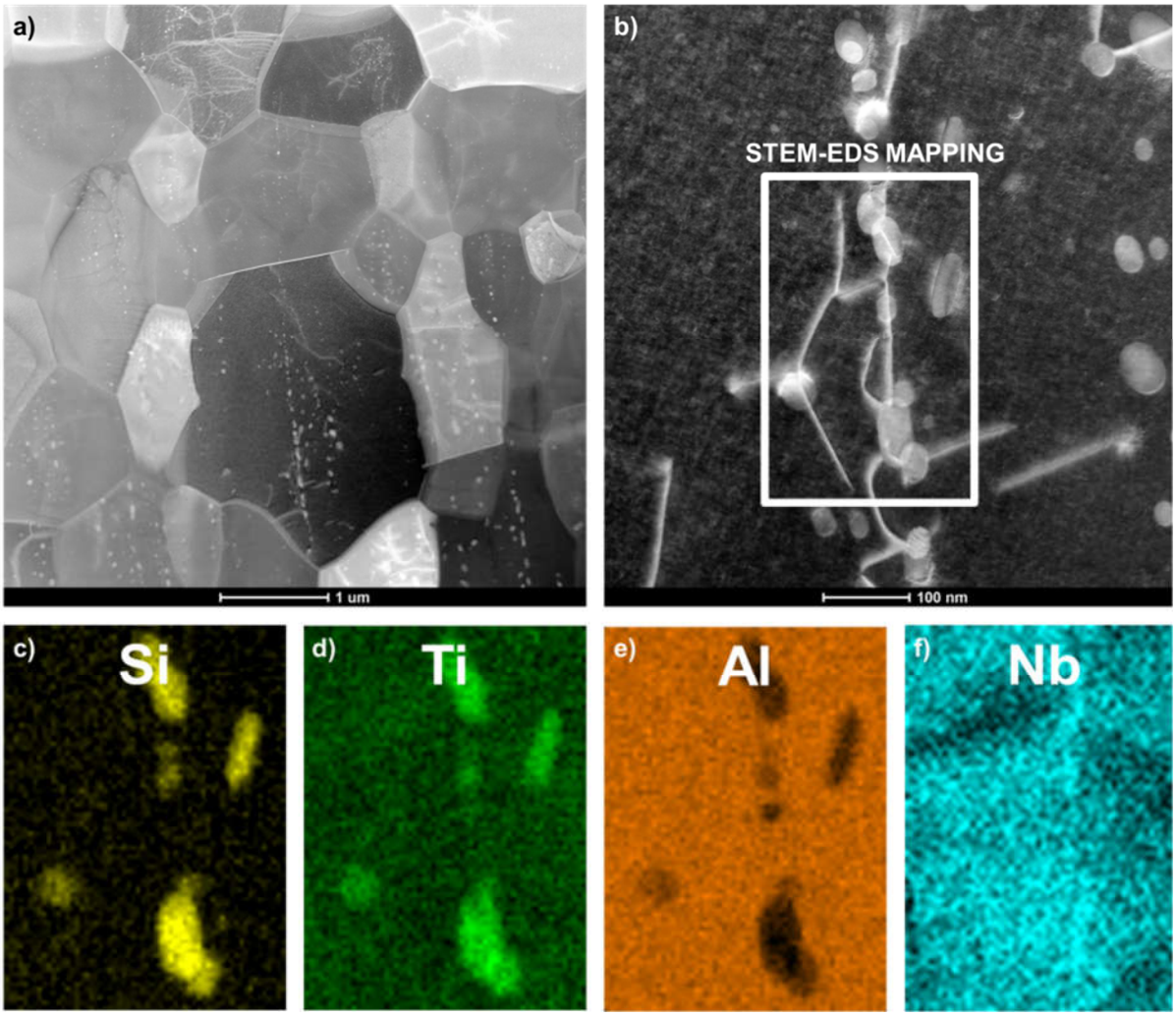

Figure 5. STEM-HAADF image of the microstructure in the outer zone of the low-Si SiAl coating (a) and b) nanometric titanium silicide precipitates within the $TiAl_3$ grains along with elemental mapping of c) Si, d) Ti, e) Al and f) Nb in the window marked in (b).

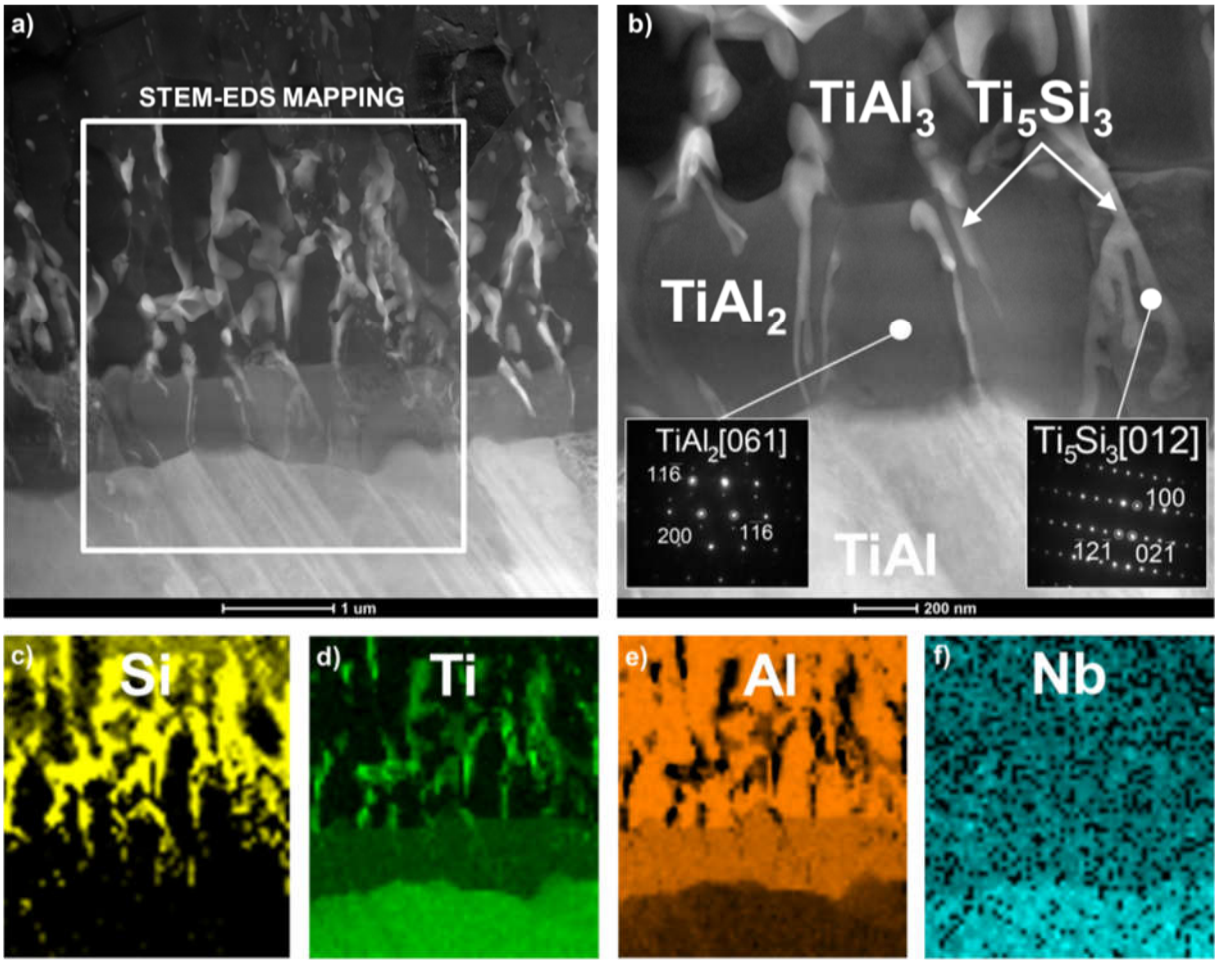

Figure 6. STEM-HAADF image of the microstructure at the interface between the low-Si SiAl coating and the substrate TiAl alloy (a) and b) intermediate $TiAl_2$ zone with elongated titanium silicide precipitates along with elemental mapping of c) Si, d) Ti, e) Al and f) Nb in the window marked in (a).

3.3. Cyclic oxidation test at 850 °C

In order to study the high temperature oxidation behavior of the simple aluminide and SiAl coatings, the cyclic oxidation test was performed at 850 °C. Moreover, for comparison purposes the cyclic oxidation behavior was also studied for the bare TiAl alloy. Based on the performed cyclic oxidation test mass change curves, in miligrams per surface area in square centimeters, were plotted as a function of the number of 23 hour cycles at 850 °C and are presented in Fig. 7. The visual appearance of all the tested samples before, during and after the cyclic oxidation test are shown in Fig. 8.

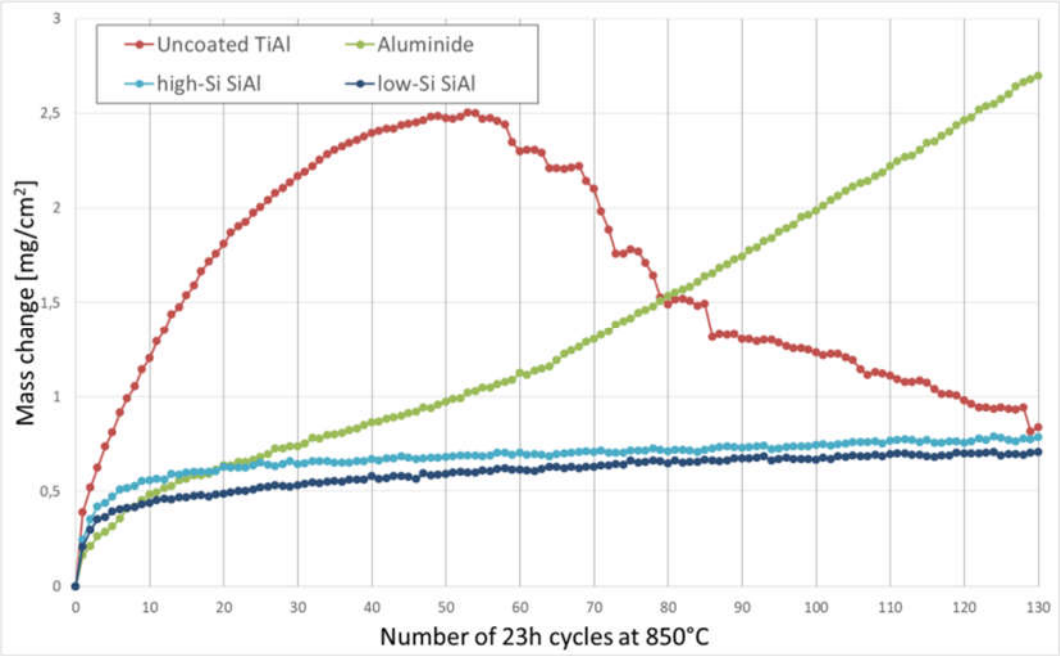

Figure 7. Mass change diagram obtained during the cyclic oxidation test at 850 °C of bare TiAl as well as TiAl with simple aluminide, low-Si and high-Si SiAl coatings.

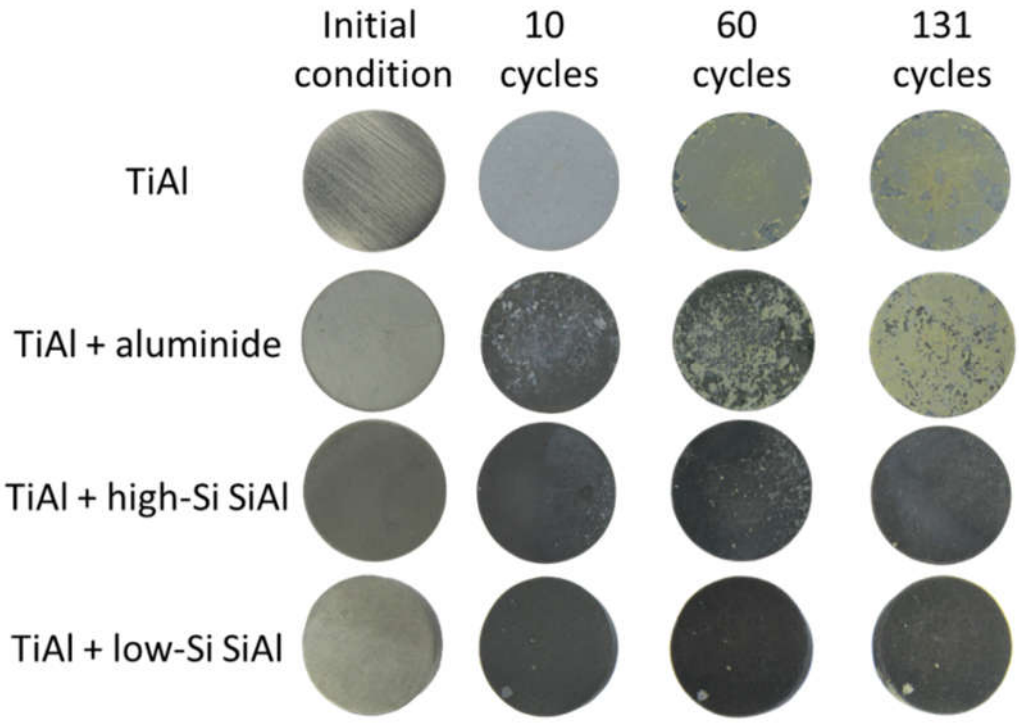

Figure 8. Visual appearance of bare TiAl and TiAl with simple aluminide, low-Si and high-Si SiAl coatings in the as-deposited condition as well as after 10, 60 and 131 23-hour cycles of oxidation at 850 °C.

The performed cyclic oxidation test revealed that the bare TiAl alloy exhibits a very rapid mass gain which reaches almost 0.5 mg/cm^2 after the 1st cycle of oxidation and then continues to increase nearly parabolically up to 2.3 mg/cm^2 after around 35 cycles, where the *n* exponent of the power law was found to be around 1.89. Moreover, the parabolic oxidation rate *kp* was calculated to be 6.91 • 10^{-3} mg^{2}cm^{-4}h^{-1}. The maximum mass gain - 2.5 mg/cm^2 was observed after around 55 cycles after which the scale spallation became dominant over its growth and rapid drops in mass occured, most certainly caused by massive scale spallation. After around 90 cycles the rate of mass loss decreases and continues up to the end of the cyclic oxidation test. However, even after 131 cycles at 850 °C the initial mass of the uncoated TiAl alloy was not reached. The surface of the uncoated TiAl sample subjected to the cyclic oxidation test, shown in the photograph in Fig. 8, reveals the grinding marks which were subsequently covered by a blue-ish oxide scale after 10 cycles. Afterwards, the oxide scale was dominated by a yellow colored oxide scale with several spallation sites on the edges of the sample, which was predominant until the end of the cyclic oxidation test at 131 cycles.

The microstructural investigations performed after the cyclic oxidation test show that the oxidation behavior of the investigated TiAl alloy is typical for this type of a material. As shown in the SEM image in Fig. 9a, after the cyclic oxidation test the surface of the sample was covered with titania (TiO_2) nodules while in the cross-section (Fig. 9b) a layered and non-protective oxide scale could be observed. It consists of the outer titania layer, intermediate titania and alumina mixture and a thin layer of Ti and Al nitrides at the metal-scale interface which is consistent with previouse published data [14,43]. The XRD results shown in Fig. 9c confirmed that during the cyclic oxidation test both TiO_2 and α-Al_2O_3 were formed along with Ti and Al nitrides, such as Ti_2AlN. The formation mechanism of such an oxide scale as well nitrided layers was described in detail in the literature [13,43–46]. Other peaks shown in Fig. 9c originate from phases present within the substrate alloy – γ-TiAl and α_2-Ti_3Al. Moreover,

based on the chemical composition results from area marked as 1 in Fig. 9b shown in Tab. 4. it is plausible that the phase directly underneath the oxide scale is γ-TiAl, as it contains around 52 at. % of Al, 45 at. % of Ti as well as Nb.

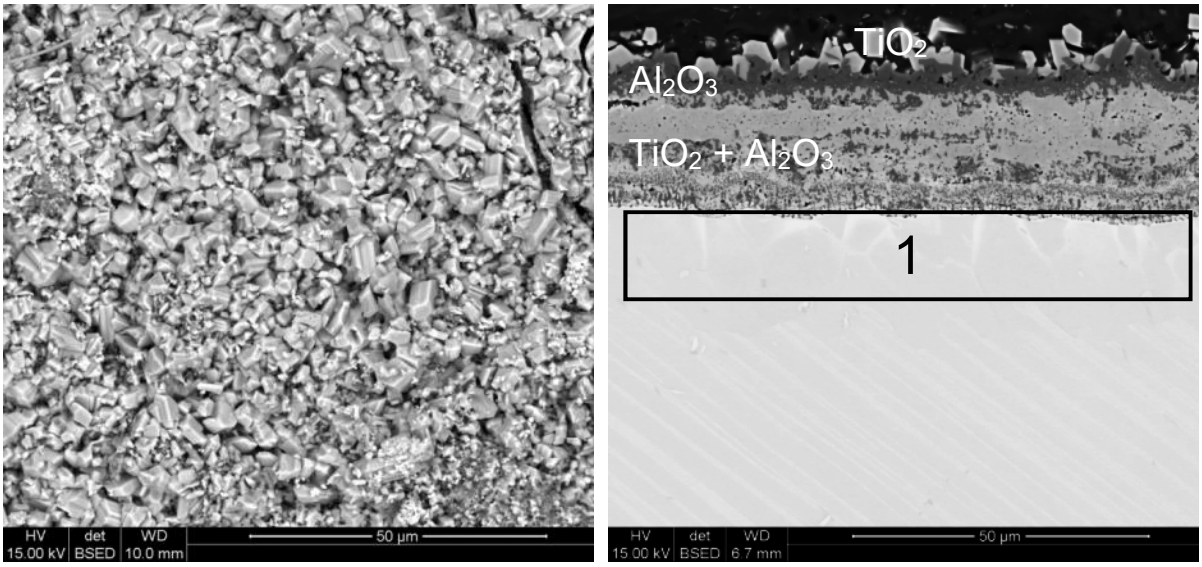

a) b)

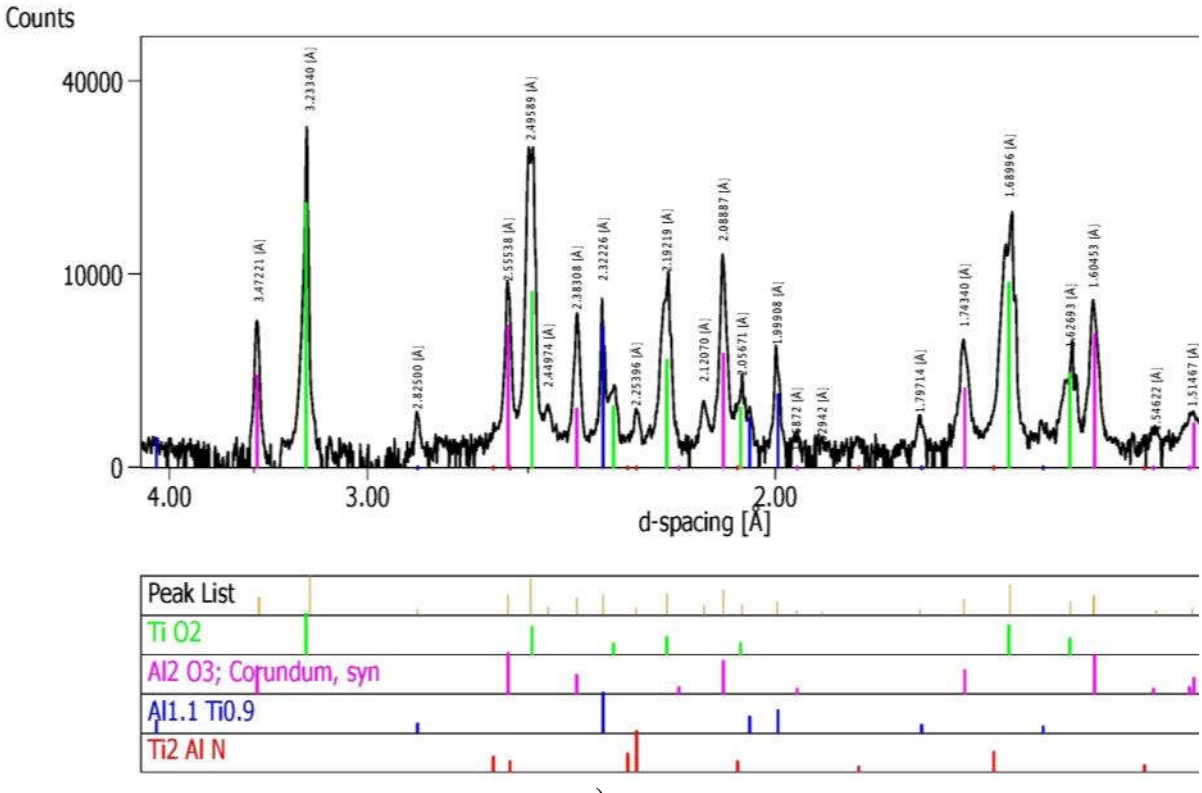

c)

Figure 9 Top view (a) and cross-sectional (b) microstructure as well as XRD pattern (c) of bare TiAl after the cyclic oxidation test at 850 °C.

Table 4 Chemical composition in microarea 1 marked in Fig. 9b.

Element	Wt %	At %
Al	33,8	50,2
Nb	13,6	5,9
Ti	52,5	43,9

Based on the mass change of the simple aluminide coatings during the cyclic oxidation test (Fig. 7) it is visible that the applied coating provides some oxidation protection up to around 60 cycles (1380 hours) at 850 °C where the oxidation rate is nearly parabolic with the *n* exponent around 2.16. The parabolic oxidation rate constant kp was calculated to be $8.14 \cdot 10^{-4}$ $mg^2cm^{-4}h^{-1}$. After this period of oxidation the mass gain increases linearly up to the end of the cyclic oxidation test, i.e. 131 cycles (3013 hours), when it reaches around 2.7 mg/cm^2. After the first 10 cycles the suraface of the sample was covered by a dark gray oxide scale, which was most likely a continuous alumina scale, with a visible formation of yellow oxides network, that possibly formed due to cracking of the coating and oxidation of the substrate alloy. By 60 cycles the yellow oxide, that is most likely titania, started to constitute the majority of the sample surface, while after the cyclic oxidaiton test (131 cycles) it was almost completely covered with them. The tetragonal $TiAl_2$ and $TiAl_3$ phases, which were observed in the as-deposited condition of the simple aluminide coating, are known for their excellent high temperature oxidation resistance [19,25,26,47]. Therefore, the coating's transition from protective to non-protective behavior at 850 °C can be explained by its relatively low thickness (around 8 μm) due to the low activity of the aluminizing process without the application of Si. The microstructural investigations performed from the surface of the coating after the 131 cycles at 850 °C (Fig. 10a) showed that it is covered with a mixture of alumina scale, characterized by a whisker-like morphology, and numerous titania nodules. The cross-sectional microstructure of the sample after the cyclic oxidation test (Fig. 10b) is similar to that observed in the bare TiAl, i.e. it is covered with a thick (> 20 μm) oxide scale (Fig. 10b). Moreover, XRD phase composition analysis (Fig. 10c) confirmed the presence of rutile (TiO_2), which is visible

as the outer layer in Fig. 10b and is also present in the middle of the oxide scale where it is mixed with alumina. Interestingly, in spite of the fact that the sample was aluminized with 100% ACP, there are no remainings of the coating after the cyclic oxidation test left, as it has been depleted due to the growth of the oxide scale as well as interdiffusion with the alloy. Moreover, the chemical composition analysis performed underneath the oxide scale revealed that it contains aroud 51 at. % of Al and 46 at. % of Ti with minor traces of Nb. This is very similar to the bare TiAl after the cyclic oxidation test where the Al content in the subsurface area was also around 52 at. %. Interestingly, phase composition analysis using XRD (Fig. 10c) showed very minor signal from $TiAl_2$ phase which is however not visible in the SEM micrograph shown in Fig. 10b. Additionally, these results indicate the presence of Ti and Al nitrides (Ti_3AlN and Ti_2AlN), that are most certainly present at the metal-scale interface, which is typical for uncoated TiAl alloys [11,13,48].

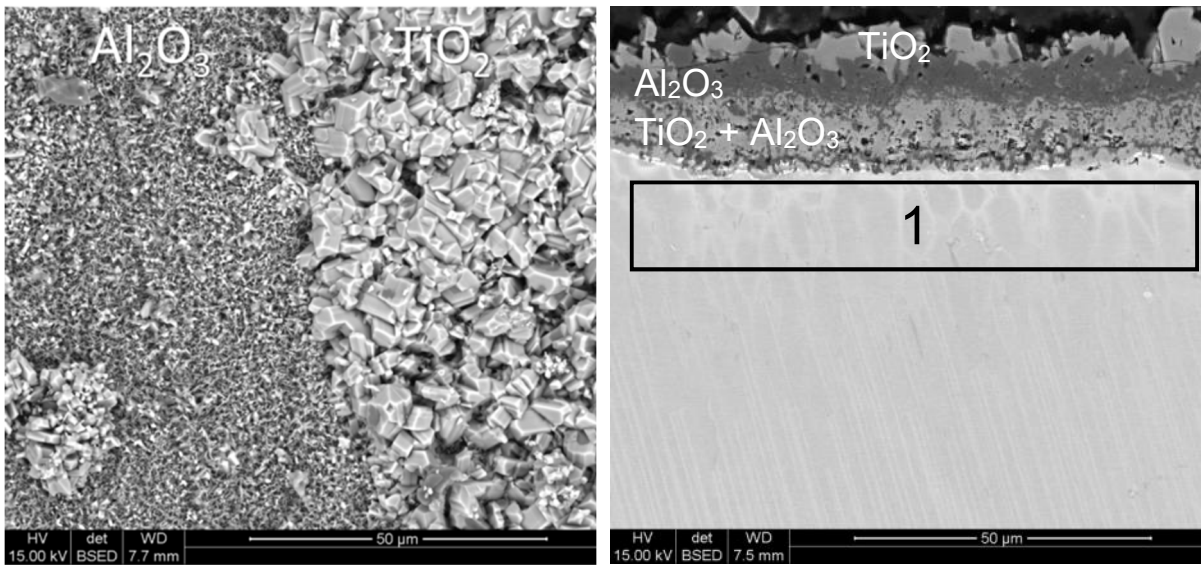

a) b)

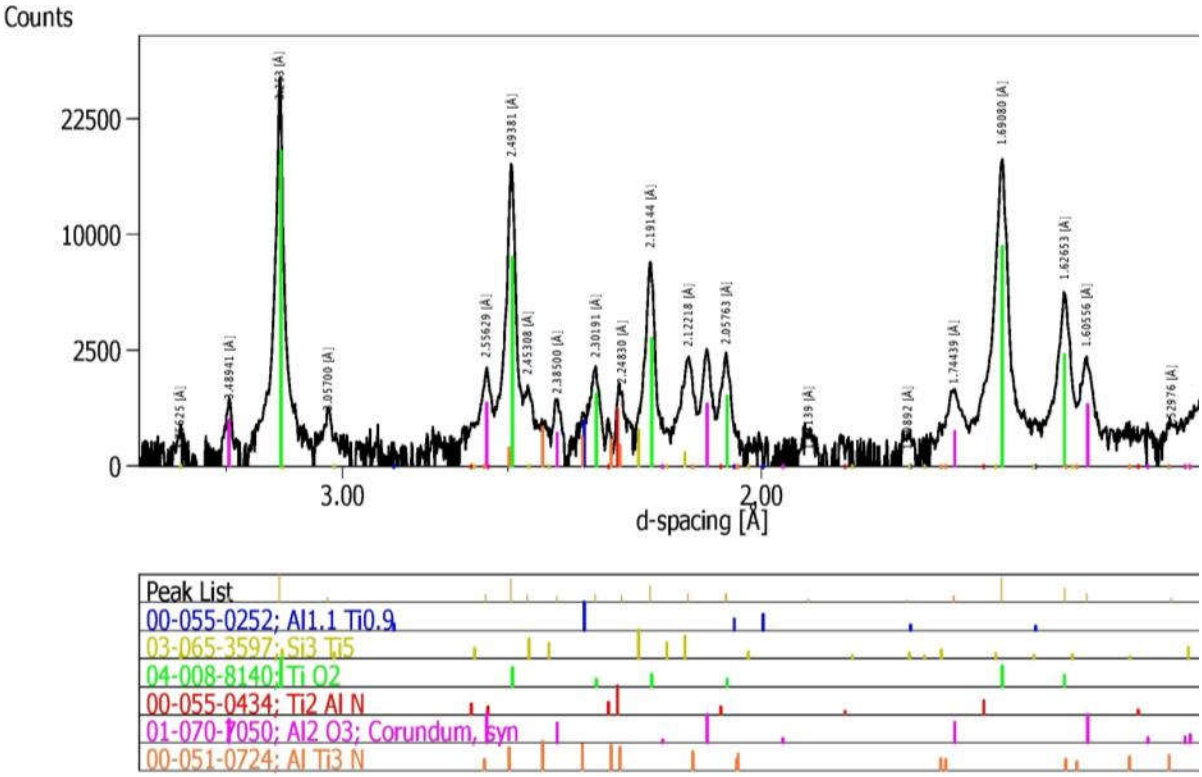

c)

Figure 10 Surface (a) and cross-sectional (b) microstructure as well as (c) XRD pattern of simple aluminide coating on TiAl after the cyclic oxidation test at 850 °C.

Table 5 Chemical composition in microarea 1 marked in Fig. 10b.

Element	wt. %	at. %
Al	35,2	51,7
Nb	13,0	5,5
Ti	51,8	42,8

As shown in the mass change diagram (Fig. 7) both the low-Si and high-Si SiAl coatings provide a significant improvement in the cyclic oxidation behavior of the coated TiAl alloy. Both coatings exhibit a quick initial mass gain to around 0.5 mg/cm^2 during the first 10 cycles at 850 °C and then oxidize very slowly according to the logarithmic law. After the 131 cycles at 850 °C the mass change of the coatings is similar – between 0.7 – 0.8 mg/cm^2. In the as-deposited condition the visual appearance of both coatings was light gray, while during the cyclic oxidation test it remained dark gray until the end of the test, which is indicative of alumina formation. Moreover, some yellow oxides were found to form at the edges of the samples, most likely Ti-oxides.

After the 131 cycles at 850 °C (3013 hours) the surface of the high-Si SiAl coating is covered by a whisker-like oxide scale (insert in Fig. 11a). In the cross-section the coating consists of an layer with around 10 µm of thickness containing an increased amount of Al – around 50 at. % along with 45 at. % Ti and Nb (marked as 1 in Fig. 11a and Tab. 6). Additionally, this zone comprises also submicron sized precipitates containing around 17 at. % Si along with 52 at. % Ti, Al and Nb. Some of the precipitates are coagulated with larger dimensions and are also segregated along the metal-scale interface. The phase composition analysis by XRD showed that the coating is composed of $TiAl_2$ as well as Ti_5Si_3 in addition to Al-enriched TiAl ($Ti_{0.9}Al_{1.1}$). The oxide scale, shown in Fig. 11b, is around 4 to 5 µm thick and is mostly composed of α-Al_2O_3, as evidenced by XRD results shown in Fig. 11c, however some peaks from TiO_2 were also found. Moreover, titanium-aluminum nitride Ti_2AlN was also detected. Similar to the as-deposited condition the XRD analysis revealed the presence of Ti_5Si_3 after the cyclic oxidation test.

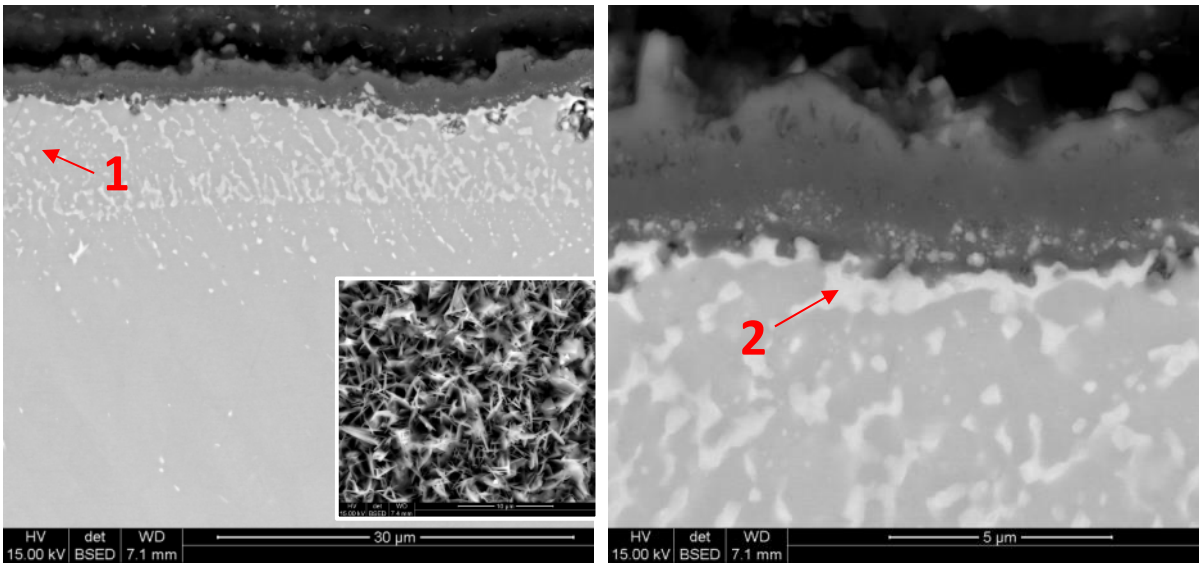

a) b)

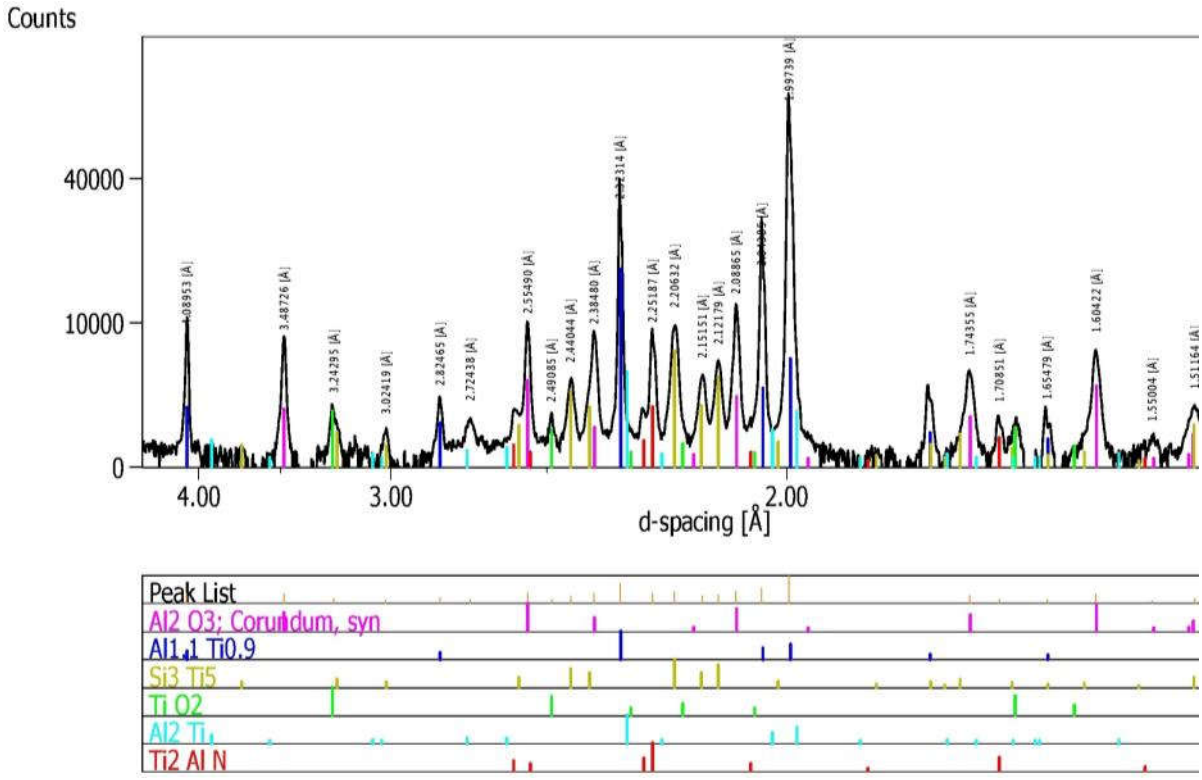

c)

Figure 11 Surface (a) and cross-sectional (a,b) microstructure of the high-Si SiAl coating on TiAl along with XRD pattern after the cyclic oxidation test at 850°C.

Table 6 Chemical composition in microareas marked in Fig. 11a,b.

Point	1		2	
Element	wt. %	at. %	wt. %	at. %
Al	33,7	49,7	17,3	26,4
Si			11,6	17,0
Nb	11,8	5,1	10,8	4,8
Ti	54,5	45,2	60,3	51,8

The STEM-HAADF image shown in Fig. 12a presents the detailed cross-sectional microstructure of the oxide scale on the high-Si SiAl coating along with its interface with the substrate. In addition to the SEM investigations shown in Fig. 11 more microstructural features are revealed such as internal porosity as well as the presence of a whisker-like outer layer along with a more continuous inner layer in the alumina scale. Moreover, the interface between the oxide scale and the substrate also contains a considerable amount of porosity in addition to numerous precipitates, visible as bright particles in the HAADF detector, which indicates

variations in the chemical composition. A more detailed microstructure of the oxide-scale interface is shown in Fig. 12b where various precipitates are visible to be mixed with the oxide scale in direct contact to the substrate. The analysis of elemental distribution in this region indicates the segregation of Si, Ti and Nb (Fig. 12c,d,g) to the bright precipitates, which were identified as Ti_5Si_3 by electron diffraction (Fig. 12h). A comparison between the Si, Ti and O (Fig. 12c,d,e) maps indicates the presence of additional precipitates, visible as light gray in Fig. 12b, that do not contain O or Si but are a mixture of Ti and Al (Fig. 12d,f). Additional STEM-EELS analysis revealed the presence of nitrogen in these precipitates (Fig. 12i) while using electron diffraction they were identified them as Ti_2AlN, which is in agreement with the XRD results shown in Fig. 11c.

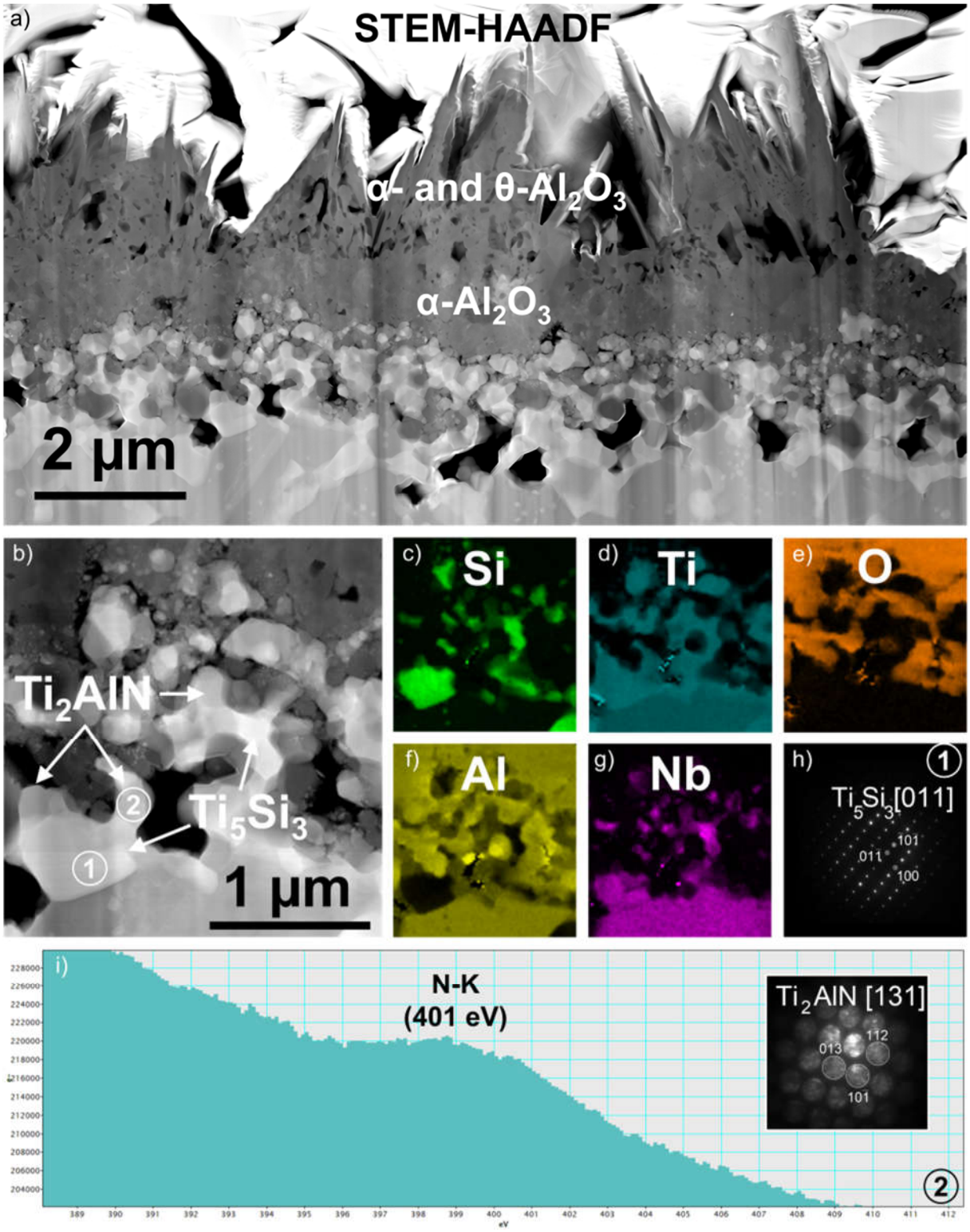

Figure 12 Cross-sectional STEM-HAADF images of the oxide scale formed on the high-Si SiAl coating on TiAl (a,b) along with elemental distribution of c) Si, d) Ti, e) O, f) Al and g) Nb after the cyclic oxidation test at 850°C, as well as electron diffraction patterns for h) Ti_5Si_3

(marked as 1) and i) Ti_2AlN along with corresponding EELS spectrum demonstrating the presence of nitrogen in the area marked as 2.

After the cyclic oxidation test the surface of the low-Si SiAl coating is similar to the previously described one, i.e. it is covered with whisker-like oxide scale, shown in the insert in Fig. 13a. However, the cross-sectional microstructure of this coating differs from the high-Si SiAl coating (Fig. 13a). As a matter of fact the coating is considerably thicker – around 27 μm, and consists of a mixture of gray and bright grains, marked as 1 and 2, respectively, in Fig. 13a. The dark areas were found to contain an increased Al content – around 66 at. % in addition to 31 at. % of Ti and Nb. Compared to that, the bright grains were rich in Ti – around 36 at. % and leaner in Al – around 59 at. %. Based on the XRD analysis results, shown in Fig. 13c, it is plausible to assume that the former grains correspond to $TiAl_2$ phase, while the latter are Al-rich TiAl phase – $Ti_{0.9}Al_{1.1}$. Moreover, the layer in the substrate, underneath the coating, was found to contain around 56 at. % Al, which also corresponds to Al-rich TiAl phase. In addition to the $TiAl_2$ and TiAl grains the coating is characterized by the presence of nanometric white precipitates distributed uniformly within it and also segregated to the metal-scale interface, marked as 4 in Fig. 13b. These precipitates were found to contian an increased Si content, as compared to the surrounding phases (Tab. 7). Moreover, based on the XRD results these precipitates are most likely Ti_5Si_3 (Fig. 13c). Furthermore, the STEM-ADF (Fig. 14a-f) and STEM-HAADF (Fig. 14g-l) investigations allowed to characterized the oxide scale as well as the metal-scale interface in more detail. The crystallographic orientation sensitive STEM-ADF (Fig. 14a) detector provides information on the size and grain shape within the studied oxide scale, while the STEM-HAADF (Fig. 14g) allows to distringuish the regions with varying chemical composition. The investigated oxide scale is around 1 μm thick and consists mostly of a continuous and compact α-Al_2O_3 with a layer of precipitates within it, which are visible in the elemental mapping of Al, O, Si, Ti and Nb in Fig. 14h-l. These precipitates were found to

contain Si, Nb and Ti and are believed to be the silicide precipitates that were present on the surface of the as-deposited coating, which were then embedded in the growing oxide scale. Furthermore, they are found to be present between the outer zone of equiaxed and slightly porous alumina grains and the inner, more columnar zone (Fig. 14a). The former was most likely formed during the initial stages of oxidation, where transient alumina polymorphs were formed, e.g. θ-Al_2O_3, and grew by outward anionic diffusion [49]. Upon the transformation of the transient θ to the more stable α polymorph the accompanying volumetric changes most likely led to formation of the porosities in this zone [50]. Moreover, at the scale-gas interface needle-like alumina can be observed, which by electron diffraction (Fig. 14c) was identified as θ-Al_2O_3 (marked as 1 in Fig. 14a). Furthermore, the inner zone of the oxide scale is composed of columnar α grains (Fig. 14d) that were formed by oxidation reaction and then grew by inward cationic diffusion (marked as 2 in Fig. 14a). The metal-scale interface contains numerous large and elongated precipitates rich in Si and Ti (marked as 3 in Fig. 14a), that were identified as Ti_5Si_3 by electron diffraction (Fig. 14e). It is also proposed that the layer of bright precipitates, rich in Si, Ti and Nb, marks the boundary between the two alumina zones that grew by different mechanisms. These precipitates were marked as 4 in Fig. 14b and identified as Ti_5Si_3, as shown in the electron diffraction pattern (Fig. 14e). As opposed to the high-Si SiAl coating, no traces of nitrides formation were found at the metal-scale interface on the low-Si SiAl coating.

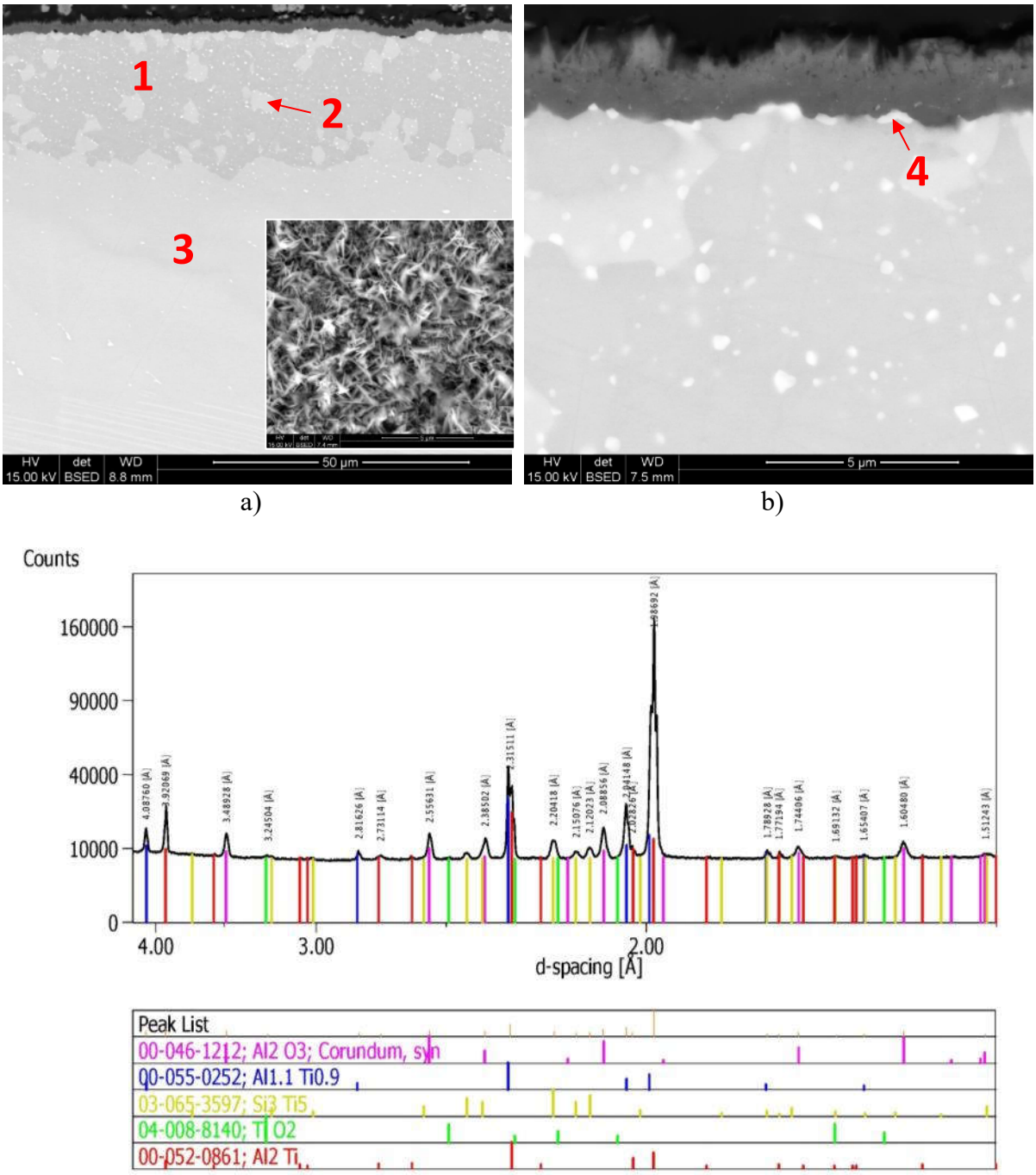

Figure 13 Surface (a) and cross-sectional (a,b) microstructure of the low-Si SiAl coating on TiAl along with XRD pattern after the cyclic oxidation test at 850°C.

Table 7 Chemical composition in microareas marked in Fig. 13a,b.

	1		2		3		4	
	wt. %	at. %	wt. %	at. %	wt. %	at. %	wt. %	at. %
Al	50,9	66,4	41,8	58,7	38,8	55,8	37,2	51,9
Si							6,0	8,0
Nb	7,1	2,7	12,6	5,1	13,4	5,6	12,0	4,8
Ti	42,0	30,9	45,6	36,1	47,8	38,6	44,8	35,2

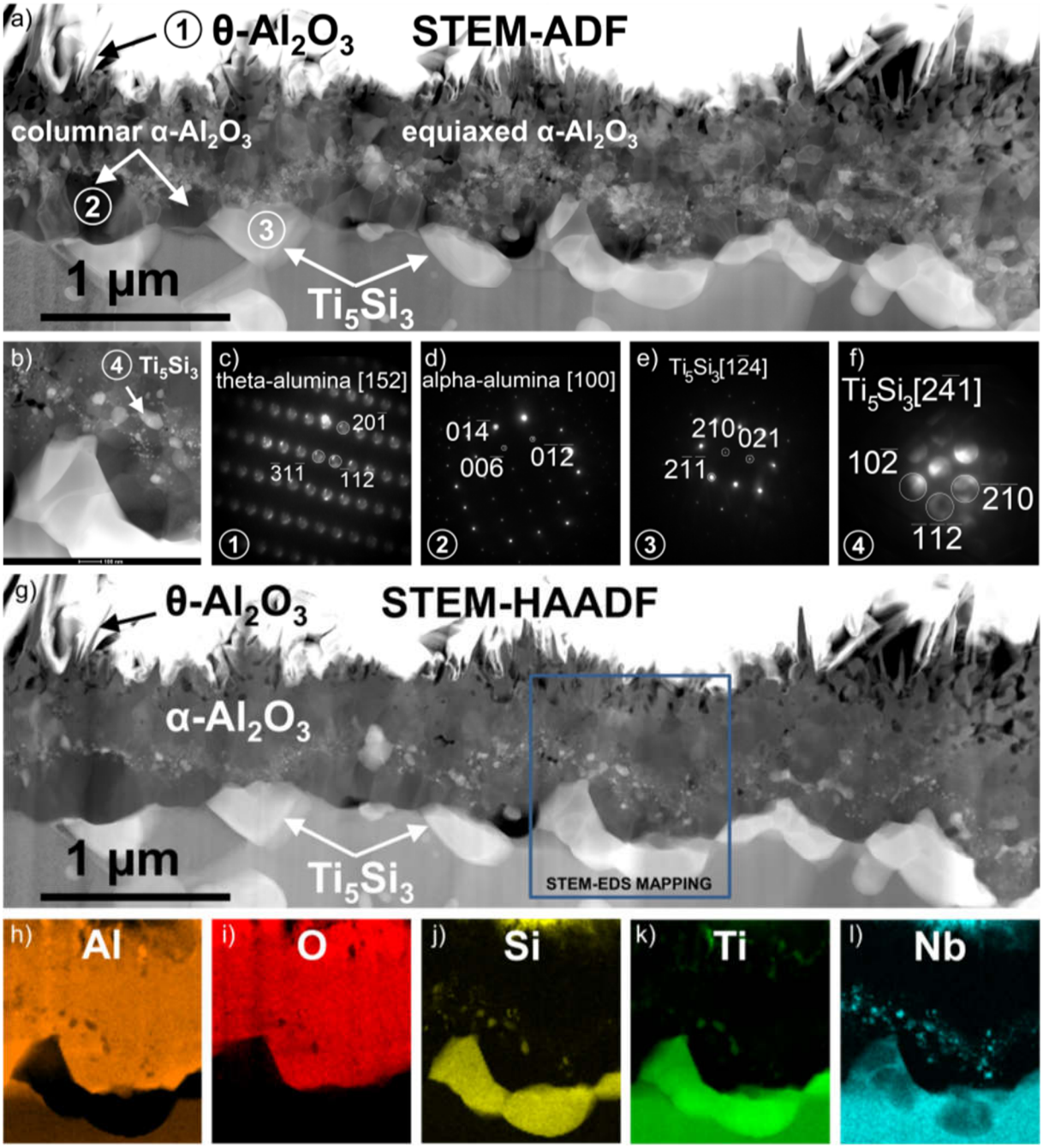

Figure 14 Cross-sectional STEM-ADF (a,b) images of the oxide scale formed on the low-Si SiAl coating on TiAl during the cyclic oxidation test at 850 °C and electron diffraction patterns for c) θ-Al_2O_3 (marked as 1), d) α-Al_2O_3 (marked as 2) and e,f) Ti_5Si_3 (marked as 3 and 4) along with STEM-HAADF image (g) with elemental mapping of h) Al, i) O, j) Si, k) Ti and l) Nb.

3.4. Discussion

The performed investigations concerning the growth of aluminide coatings on γ-TiAl indicate a strong influence of the powder composition on the thickness, as well as chemical and phase composition of the obtained coatings. It has been demostrated that the application of 100% ACP powder in the pack cementation process without Si leads to a relatively low thickness of the coating (around 8 μm). This is most likely related to the low activity of the process where the gradient of Al between the reactive atmosphere and the somewhat Al-rich TiAl alloy is too low to be the driving force for its inward diffusion. Nonetheless, this thin aluminide coating is composed of the $TiAl_3$ and $TiAl_2$ phases and contains around 75 at. % of Al in its outer zone. It has been found that when the ACP is mixed with silicon in various proportions the activity of the process increases significantly. It has been shown that increasing the addition of ACP to silicon powder results in an increase of coating thickness and formation of a double-layered microstructure, the majority of which is the $TiAl_3$ phase, with very thin $TiAl_2$ phase formation underneath it, which is in agreement with investigations of SiAl coatings obtained using Arc-PVD [23,24] or slurry methods [25]. Consequently, the amount of titanium silicides decreases with increasing ACP content in the powder. There is most likely an interplay between the Al and Si within the pack that leads to an increased activity of the process. It is suggested to be related to the tendency of Si and Al to format low temperature melting eutectics, such as e.g. 12Al-Si melting at 577 °C [51]. Assuming that at 850 °C some part of the coating deposition process may occur from the liquid phase could explain the increased coating growth rate when both Si and Al are present in the pack. It is interesting to note that the coating consists mainly of aluminides, and only minor amounts of silicides are present within it. It is most likely due to the fact that the partial pressures of gaseous aluminium halides (such as AlCl, $AlCl_2$, $AlCl_3$) are much higher compared to those of Si (SiCl, $SiCl_2$, $SiCl_3$, $SiCl_4$) [52].

The relatively low thickness of the simple aluminide coating translates to a fairly high oxidation resistance up to 60 cycles, where the oxidation proceeds by near-parabolic law and the oxidation rate constant is almost 8.5x lower than that of the bare alloy. However, the Al depletion, due to oxide scale growth and interdiffusion with the substrate alloy, leads to a nearly linear oxidation kinetics upon further exposure. After the cyclic oxidation test the oxide scale is composed of a mixture of titania and alumina, with formation of Ti and Ti-Al nitrides at the metal-scale interface, which is similar to the investigated uncoated TiAl and other alloys of this type [14,43,53].

The aluminide coatings modified with Si also suffer from Al depletion at 850 °C, due to interdiffusion as well as growth of the oxide scale. Especially during the first 5 cycles the coatings showed a higher mass gain than the pure aluminide coating. This could result from the formation of the fast growing and metastable θ-Al_2O_3 [54]. In fact, after oxidation the outer layer of the oxide scale formed on both SiAl coatings still contained some whisker-like θ-Al_2O_3, which was not observed in our previous study performed at higher temperature – 950 °C [19]. Gauthier et al. [47] observed that at certain temperatures $TiAl_3$ is prone to form θ-Al_2O_3 and thus a thicker oxide layer, whereas $TiAl_2$ forms a stable α-Al_2O_3 scale. In other intermetallic systems, such as NiAl and FeAl, the addition of Cr [55,56] or rare earth elements like Y and Ce [57] have an effect on the formation of θ-Al_2O_3. The available literature does not provide information about the effect of Si and silicide in $TiAl_3$ on the formation of θ-Al_2O_3. However, based on the STEM investigations of the studied coatings after the cyclic oxidation test it was found that silicon segregated to the metal-scale interfaces and formed precipitates much larger compared to the as-deposited condition. This ripening of the silicide precipitates is suggested to result from the Ti being captured by Si from the $TiAl_3$ and $TiAl_2$ phases upon their oxidation and simultaneous loss of Al to form the Al_2O_3 scale. During the initial stages of oxidation this effect could be disadvantageous since the $TiAl_3$ phase is stabilized and therefore the growth of

θ-Al_2O_3 is prolonged. However, during further oxidation the θ-Al_2O_3 formed during the initial stages of oxidation transforms to the stable α-Al_2O_3. Moreover, underneath the transformed region new columnar α-Al_2O_3 grains nucleate and grow. For example, the studies of (Ni,Pt)Al oxidation behavior showed that the thickness of the whisker like θ-Al_2O_3 can be used to estimate chronological order of the θ to α transformation [58]. Since the high-Si SiAl coating has more pronounced whisker like θ-Al_2O_3 compared to the low-Si SiAl it can be assumed that the formation of α-Al_2O_3 occurred later, which is in agreement with the higher mass gain during the initial stages of oxidation. However, after around 50 cycles of oxidation the growth rates are comparable for both Si contents indicating comparable mechanism during further oxidation. Besides the capturing effect of Si, the Ti_5Si_3 has a coefficient of thermal expansion (CTE) which is comparable to that of Al_2O_3 [59] and therefore could prevent cracking and spallation of the oxide scale during cyclic oxidation [60]. However, it was found that after the cyclic oxidation test, i.e. 131 cycles of 23 hour duration each (3013 hours of dwell time in total at 850 °C), the mass gain of both coatings remained very low (0.7 – 0.8 mg/cm^2). The results of long-term oxidation tests at 850 °C that could be found in the literature concerned the application of coatings such as CrAlYN/CrN produced by magnetron sputtering (~1.3 mg/cm^2 after 2000 h) or HIPIMS (~0.8 mg/cm^2 after 2000 h) [61], CrAlN-YN (0.8 mg/cm^2 after 2000 h) [18], halogen effect (1 mg/cm^2 after 4000 h at 900 °C) [62], TiCrAlY (0.4 mg/cm^2 after 1000 h at 850 °C) [39] or TiCrAlZr + 7YSZ (0.6 mg/cm^2 after 2000 h at 850 °C). After the cyclic oxidation test the surface of both SiAl coatings studied in this work was covered with a continuous and very thin α-Al_2O_3 scale. The obtained results indicate that an increase of around 7 µm in the aluminide coating results in a lower mass gain and provides a high amount of Al-rich $TiAl_2$ phase after over 3000 hours of exposure. Compared to that, the thinner coating obtained with higher amount of Si contains only minor amounts of $TiAl_2$ after the cyclic oxidation test and is mostly composed of Al-rich TiAl phase with silicide precipitates. The gradual decrease in Al

content and subsequent transformation from $TiAl_3$ through $TiAl_2$ to TiAl was observed also by others [31,63]. Based on the STEM investigations of the studied coatings after the cyclic oxidation test it was found that silicon segregated to the metal-scale interfaces and formed precipitates much larger compared to the as-deposited condition. This ripening of silicide precipitates is suggested to result from the Ti being captured by Si from the $TiAl_3$ and $TiAl_2$ phases upon their oxidation and simultaneous loss of Al to form the Al_2O_3 scale. Other works reported [20] that silicide coatings on γ-TiAl provide excellent oxidation resistance at 950 °C when they are composed of Ti_5Si_3, however the oxide scales they formed were mainly composed of $TiO_2 + SiO_2 + Al_2O_3$. Moreover, Tang et al. [64,65] demonstrated the propensity of Ti_5Si_3 for formation of TiN when the pO_2 is very low, i.e. below ~10^{-30} Pa. Additionally they showed that the oxidation behavior of Ti_5Si_3 is very sensitive to its stoichiometry – Si-rich $Ti_5Si_{3.2}$ demonstrates much lower mass gains compared to Ti-rich $Ti_5Si_{2.8}$ at 1000 °C. It is interesting to note that the STEM-HAADF investigations did not reveal any formation of Si or Ti oxides on any of the SiAl coatings, although the silicide precipitates, identified as Ti_5Si_3, were found to be present at the metal-scale interface. In the case of the Al-leaner coating (high-Si SiAl), the Ti_5Si_3 precipitates were found to form Ti_2AlN, while on the low-Si SiAl coating no nitrides were found and alumina scale formed on the silicides. Based on the Ti-Al-Si equilibrium diagram [66] it is found that Ti_5Si_3 has a limited solubility of Al of around 6 at. %. Based on the mentioned literature data and the results obtained in this work it is suggested that the partial pressure of oxygen underneath the continuous alumina scale was too low to oxidize either Ti or Si from the Ti_5Si_3, thus only alumina was found to form. Moreover, when the Al is depleted to a certain level, both in the silicides and the coating, the former tend to react with nitrogen to form Ti-Al nitrides in the low pO_2 underneath the oxide scale.

4. Summary

The presented work demonstrates the influence of Si and its content on the growth and oxidation behavior of aluminide coatings on the TiAl-based alloy TNB-V5. The results clearly show that the application of Si-free aluminium containing powder (ACP) provides a low Al activity during the deposition process resulting in a low thickness of the coating. The obtained coating remains protective up to around 60 cycles (total of 1380 hours) at 850 °C. The application of Si and ACP in the coating deposition process results in a significant increase in coatings thickness of up to 36 µm leading to a very low mass gain of around 0.7-0.8 mg/cm^2 during 131 cycles (3013 hours) at 850 °C. STEM investigations of the oxide scales after the cyclic oxidation test indicated large differences in oxide scale formation. While Si-free coatings developed thick and non-protective mixed titania-alumina scales, the formation of continuous and very thin α-Al_2O_3 scales was observed for Si-modified coatings (4 µm for the high-Si and 1 µm for the low-Si SiAl coating). Moreover, segregation and ripening of silicide precipitates at the metal-scale interface was observed during long-term exposure at 850 °C. It has been found that the Ti silicides, due to their limited solubility of Al, are capable of forming alumina scale without silica or titania. However, upon Al depletion, Ti-Al nitrides are formed in the low pO_2 present underneath the continuous alumina scale. Both Si levels provided excellent oxidation protection of the TNB TiAl alloy up to more than 3000h without any major degradation of the coatings and no attack of the base material.

Acknowledgements

The authors would like to thank Mr W. Supernak for the support with technological experiments, Dr. H. Krztoń for the XRD measurements and Mr P. Stawarczyk for sample preparation.

This work was sponsored by the National Science Centre, Poland under contract UMO-2016/23/G/ST5/04128 and of Deutsche Forschungsgemeinschaft (DFG), Germany under contract Schu1372/6-1 within the Beethoven II programme - TiAlMET project.

5. Literature

[1] Y.W. Kim, JOM 46 (1994) 30–39.

[2] T. Tetsui, S. Ono, Intermetallics 7 (1999) 689–697.

[3] B.P. Bewlay, S. Nag, A. Suzuki, M.J. Weimer, TiAl Alloys in Commercial Aircraft Engines, Taylor & Francis, 2016.

[4] U. Habel, F. Heutling, K. C., W. Smarsly, G. Das, H. Clemens, Proc. 13th World Conf. Titanium, San Diego, CA, USA, John Wiley Sons, Inc. (2016) 1223–1227.

[5] T. Klein, H. Clemens, S. Mayer, Materials (Basel). 9 (2016) 755.

[6] Y.W. Kim, S.L. Kim, Jom 70 (2018) 553–560.

[7] M.P. Brady, W.J. Brindley, J.L. Smialek, I.E. Locci, Jom 48 (1996) 46–50.

[8] E.A. Loria, Intermetallics 8 (2000) 1339–1345.

[9] E.A. Loria, Intermetallics 9 (2001) 997–1001.

[10] R. Pflumm, S. Friedle, M. Schütze, Intermetallics 56 (2015) 1–14.

[11] F. Dettenwanger, E. Schumann, M. Ruhle, J. Rakowski, G. Meier, Oxid. Met. 50 (1998) 269–307.

[12] M. Schütze, JOM 69 (2017) 2602–2609.

[13] J.M. Rakowski, F.S. Pettit, G.H. Meier, F. Dettenwanger, E. Schumann, M. Ruhle, Scr. Metall. Mater. 33 (1995) 997–1003.

[14] R. Swadźba, K. Marugi, Pyclik, Corros. Sci. 169 (2020) 108617.

[15] Y. Xiong, S. Zhu, F. Wang, Surf. Coatings Technol. 197 (2005) 322–326.

[16] M. Moser, P.H. Mayrhofer, H. Clemens, Intermetallics 16 (2008) 1206–1211.

[17] S. Sarkar, S. Datta, S. Das, D. Basu, Surf. Coatings Technol. 203 (2009) 1797–1805.

[18] R. Braun, F. Rovere, P.H. Mayrhofer, C. Leyens, Intermetallics 18 (2010) 479–486.

[19] R. Swadźba, L. Swadźba, B. Mendala, B. Witala, J. Tracz, K. Marugi, Pyclik, Intermetallics 87 (2017) 81–89.

[20] M. Fröhlich, A. Ebach-Stahl, R. Braun, C. Leyens, Materwiss. Werksttech. 38 (2007) 667–673.

[21] S. Gong, H. Xu, Q. Yu, C. Zhou, Surf. Coatings Technol. 130 (2000) 128–132.

[22] W. Liang, X.X. Ma, X.G. Zhao, F. Zhang, J.Y. Shi, J. Zhang, Intermetallics 15 (2007) 1–8.

[23] L. Swadzba, G. Moskal, M. Hetmanczyk, B. Mendala, G. Jarczyk, Surf. Coatings Technol. 184 (2004) 93–101.

[24] L. Swadzba, A. Maciejny, B. Mendala, G. Moskal, G. Jarczyk, Surf. Coatings Technol. 165 (2003) 273–280.

[25] M. Goral, L. Swadzba, G. Moskal, M. Hetmanczyk, T. Tetsui, Intermetallics 17 (2009) 965–967.

[26] M. Goral, L. Swadzba, G. Moskal, G. Jarczyk, J. Aguilar, Intermetallics 19 (2011) 744–747.

[27] D.J. Kim, D.Y. Seo, X. Huang, Q. Yang, Y.W. Kim, Surf. Coatings Technol. 206 (2012) 3048–3054.

[28] C. Zhou, H. Xu, S. Gong, K. Young Kim, Mater. Sci. Eng. A 341 (2003) 169–173.

[29] S.B. Abu Suilik, K. Takeshita, H. Kitagawa, T. Tetsui, K. Hasezaki, Intermetallics 15 (2007) 1084–1090.

[30] C.G. Zhou, H.B. Xu, S.K. Gong, Acta Metall. Sin. (English Lett. 13 (2000) 1148–1154.

[31] R. Braun, M. Fröhlich, C. Leyens, D. Renusch, Oxid. Met. 71 (2009) 295–318.

[32] A. Szkliniarz, G. Moskal, W. Szkliniarz, R. Swadźba, Surf. Coatings Technol. 277 (2015) 270–277.

[33] A. Donchev, E. Richter, M. Schütze, R. Yankov, J. Alloys Compd. 452 (2008) 7–10.

[34] M. Schütze, G. Schumacher, F. Dettenwanger, U. Hornauer, E. Richter, E. Wieser, W. Möller, Corros. Sci. 44 (2002) 303–318.

[35] S. Friedle, N. Nießen, R. Braun, M. Schütze, Surf. Coatings Technol. 212 (2012) 72–78.

[36] N. Laska, S. Friedle, R. Braun, M. Schütze, Mater. Corros. (2016) 1–10.

[37] N. Laska, R. Braun, Oxid. Met. 81 (2014) 83–93.

[38] R. Braun, M. Fröhlich, W. Braue, C. Leyens, Surf. Coatings Technol. 202 (2007) 676–680.

[39] N. Laska, R. Braun, S. Knittel, Surf. Coatings Technol. 349 (2018) 347–356.

[40] A. Lange, R. Braun, M. Heilmaier, Intermetallics 48 (2014) 19–27.

[41] N. Laska, S. Friedle, R. Braun, M. Schütze, Mater. Corros. 67 (2016) 1185–1194.

[42] M. Fröhlich, R. Braun, C. Leyens, Surf. Coatings Technol. 201 (2006) 3911–3917.

[43] F. Dettenwanger, E. Schumann, M. Ruhle, J. Rakowski, G. Meier, Oxid. Met. 50 (1998) 269–307.

[44] W. Lu, C. Chen, Y. Xi, C. Guo, F. Wang, L. He, Intermetallics 15 (2007) 824–831.

[45] M. Yoshihara, K. Miura, Intermetallics 3 (1995) 357–363.

[46] G.H. Meier, F.S. Pettit, S. Hu, Le J. Phys. IV 03 (1993) C9-395-C9-402.

[47] V. Gauthier, F. Dettenwanger, M. Sch??tze, V. Shemet, W.J. Quadakkers, Oxid. Met. 59 (2003) 233–255.

[48] W.J. Quadakkers, P. Schaaf, N. Zheng, A. Gil, E. Wallura, Oxid. Intermet. (2007) 275–287.

[49] G. Rybicki, J.L. Smialek, Oxid. Met. 31 (1989) 275–304.

[50] B.A. Pint, Oxid. Met. 48 (1997) 24–27.

[51] J.L. Murray, A.J. McAlister, Bull. Alloy Phase Diagrams 5 (1984) 74–84.

[52] R. Bianco, M.A. Harper, R.A. Rapp, Jom 43 (1991) 68–73.

[53] I. Abdallah, C. Dupressoire, L. Laffont, D. Monceau, A. Vande Put, Corros. Sci. 153 (2019) 191–199.

[54] H.J. Grabke, Intermetallics 7 (1999) 1153–1158.

[55] R. Klumpes, C.H.M. Marée, E. Schramm, J.H.W. de Wit, Mater. Corros. 47 (1996) 619–624.

[56] M.W. Brumm, H.J. Grabke, 33 (1992) 1677–1690.

[57] I. Rommerskirchen, V. Kolarik, Oxid. Intermet. 47 (2007) 109–120.

[58] V.K. Tolpygo, D.R. Clarke, (n.d.) 59–70.

[59] W. Liang, X.X. Ma, X.G. Zhao, F. Zhang, J.Y. Shi, J. Zhang, Intermetallics 15 (2007) 1–8.

[60] T.L. K. Bobzin, T. Brögelmann, C. Kalscheuer, Surf. Coat. Technol. 350 (2018) 587–595.

[61] R. Braun, U. Schulz, C. Leyens, P.E. Hovsepian, A.P. Ehiasarian, Int. J. Mater. Res. 101 (2010) 648–656.

[62] H.E. Zschau, M. Schütze, H. Baumann, K. Bethge, Nucl. Instruments Methods Phys. Res. Sect. B Beam Interact. with Mater. Atoms 240 (2005) 137–141.

[63] M.S. Chu, S.K. Wu, Oxid. Met. 63 (2005) 1–13.

[64] Z. Tang, J.J. Williams, A.J. Thom, M. Akinc, Intermetallics 16 (2008) 1118–1124.

[65] Z. Tang, A.J. Thom, M. Akinc, Intermetallics 14 (2006) 537–543.

[66] Z. Li, C. Liao, Y. Liu, X. Wang, Y. Wu, M. Zhao, Z. Long, F. Yin, J. Phase Equilibria Diffus. 35 (2014) 564–574.